

Rapid Determination of Trace Element Compositions in Peridotites by LA-ICP-MS Using an Albite Fusion Method

Shenyang Y. Zhang (1), Hongluo L. Zhang (1)* , Zhenhui Hou (1), Dmitri A. Ionov (2, 3) and Fang Huang (1)*

(1) CAS Key Laboratory of Crust-Mantle Materials and Environments, School of Earth and Space Sciences, University of Science and Technology of China, Hefei, 230026, Anhui, China

(2) Géosciences Montpellier, Université de Montpellier, Montpellier, 34095, France

(3) State Key Laboratory of Isotope Geoscience, Guangzhou Institute of Geochemistry, Guangzhou, 510640, Guangdong, China

* Corresponding author. e-mails: hongluo@ustc.edu.cn and fhuang@ustc.edu.cn

A rapid sample preparation procedure is described to determine trace element compositions of peridotites using LA-ICP-MS. Peridotite powders were fused with albite in a molybdenum–graphite assembly to obtain homogeneous glasses. Best conditions for the fusion procedure (heating at 1500–1550 °C for 10–15 min with a sample-to-flux ratio of 1:2) were constrained with melting experiments on two USGS reference materials, PCC-1 and DTS-2B. Mass fractions of first series transition elements, Ba and Pb, in quenched glasses of PCC-1 and DTS-2B are consistent with published data within 10% RSD. Three spinel peridotite xenoliths from eastern China were analysed following both our method and conventional solution ICP-MS. Compared with solution ICP-MS, the relative deviations of our method for most elements were within 10%, while for the REE, Ta, Pb, Th and U, the relative deviations were within 20%. In particular, volatile elements (e.g., Pb and Zn) are retained in the glass. Compared with conventional wet chemistry digestion, our method is faster. Additional advantages are complete sample fusion, especially useful for samples with acid-resistant minerals (spinel and rutile), and long-term conservation of glasses allowing unlimited repeated measurements with microbeam techniques. The same approach can be used for analyses of other mantle rocks, such as eclogites and pyroxenites.

Keywords: trace elements, peridotite, LA-ICP-MS, albite fusion, microbeam analyses.

Received 11 Apr 18 – Accepted 25 Aug 18

Peridotites are the dominant rocks of the Earth's upper mantle at depths down to > 200 km. Data on chemical compositions of peridotites are essential to constrain the origin and evolution of the lithospheric mantle and the silicate Earth (McDonough 1990, Bodinier and Godard 2014, Pearson *et al.* 2014). The abundances of trace elements in mantle materials, in particular, provide important insights into the fractionation of the Earth's deep interior involving partial melting and metasomatism (e.g., Frey and Prinz 1978, Rampone *et al.* 1996, Foley *et al.* 2002, Ionov *et al.* 2002).

Major advances in the knowledge of trace element abundances in mantle peridotites are related to the application of solution inductively coupled plasma-mass spectrometry (ICP-MS; e.g., Jenner *et al.* 1990). A prerequisite for using this technique to analyse bulk rock samples,

however, is acid digestion of rock powders followed by a series of wet chemistry procedures (e.g., Ionov *et al.* 1992, Jarvis 1992). These procedures are time-consuming, require dangerous, highly concentrated acids and must be done in a clean laboratory environment. A general concern with the acid attack is the formation of insoluble fluorides by reaction with HF. A particular problem with digestion of peridotites is the common presence of acid-resistant minerals, such as Cr-Al spinel as well as occasional accessory phases of metasomatic origin, for example, rutile and other Ti-rich oxides (Ionov *et al.* 1999). More or less complete dissolution of such phases can be achieved using pressurised containers (e.g., Cotta and Enzweiler 2012), combinations of acid mixtures (e.g., Yokoyama *et al.* 1999) or fusion or sintering rock powders with alkalis before dissolution (e.g., Bayon *et al.* 2009, Bokhari and Meisel 2017).

Another conundrum in determining trace elements using solution ICP-MS is the high mass fraction of major elements (e.g., Fe and Mg for peridotites) in the solution (matrix effects) that can lead to a reduction in trace element signal intensities or to a partial blockage of the orifices, thus reducing the ion supply into the mass spectrometer (Kawaguchi *et al.* 1987, Makishima and Nakamura 1997). Chemical methods developed to overcome these effects (coprecipitation and ion exchange) are complicated and allow determining only a limited number of elements (Barrat *et al.* 1996, Qi *et al.* 2005, Sun *et al.* 2013, Rospabé *et al.* 2018). We show below that some of the matrix effects are easier to take into account using our fusion method.

Fusion of peridotite powders with alkali salts (LiBO_2 , $\text{Li}_2\text{B}_4\text{O}_7$, Na_2CO_3 , NaOH and Na_2O_2), a common procedure to produce glass beads for major element analyses by X-ray fluorescence (XRF), may assure complete subsequent sample dissolution (e.g., Eggins 2003, Bayon *et al.* 2009). However, the samples must be highly diluted due to the use of high mass proportions of flux agents such that the mass fractions of trace elements may be driven below detection limits (Yu *et al.* 2003). In addition, the flux inevitably contaminates ICP-MS instruments with Li and B (Meisel *et al.* 2002).

Pressed powder pellets have been widely used to determine major and trace element mass fractions of silicate samples (e.g., Gray 1985, Zhu *et al.* 2013b, Mukherjee *et al.* 2014). However, the analytical precision of this method is not sufficiently high [normally about 10–20% relative standard deviation (RSD)] due to sample inhomogeneity, which may be caused by sample grain size (Mukherjee *et al.* 2014, Tabersky *et al.* 2014). To improve sample homogeneity, Garbe-Schönberg and Müller (2014) and Peters and Pettke (2017) produced nanoparticulate pressed powder pellets via well-milling, which were successfully applied to bulk analysis of the serpentine UB-N and the peridotite JP-1, with precision below 5% RSD. However, the grinding procedure is time-consuming and may imply contamination and loss of elements (e.g., Ni, Cu and Zn; Zhang *et al.* 2016).

An alternative to the solution ICP-MS analyses and pressed powder pellet technique is producing homogeneous glass beads from rock powders for *in situ* analyses by laser ablation (LA) ICP-MS, with matrix effects corrected using ablation yield correction factor and reference glasses as multiple reference materials (Liu *et al.* 2008, Chen *et al.* 2011). For some rocks, flux-free fusion techniques have been applied successfully avoiding contamination from the flux (e.g., Fedorowich *et al.* 1993). Rock samples are normally

melted at 1300–1800 °C using an iridium strip heater (Stoll *et al.* 2008) or a high-temperature furnace in a platinum and boron nitride crucible (Kurosawa *et al.* 2006, Zhu *et al.* 2013a, Bao *et al.* 2016). Although such methods are simple and rapid, using iridium strip heaters could cause a loss of volatile elements (e.g., Pb, Zn and Cs) due to the high temperature (Stoll *et al.* 2008), whereas transition metals (Cr, Ni and Cu) may migrate out of the melt when using platinum and boron nitride crucibles (Kurosawa *et al.* 2006, Zhu *et al.* 2013a, Bao *et al.* 2016). Importantly, such methods cannot be applied to peridotites due to their high liquidus temperatures (e.g., 1725 ± 30 °C, at 1 bar for garnet-lherzolite, Carswell 1968, 1850 °C, at 1 bar for dunite, Herzberg 1983), which cannot be achieved by normal furnaces. Furthermore, peridotite melts cannot be quenched to homogeneous glass due to high MgO concentrations, which lead to nucleation of olivine and other minerals (e.g., Takahashi and Kushiro 1983).

In this study, we establish a new sample preparation method to analyse trace element mass fractions in peridotites by LA-ICP-MS. To turn peridotite into homogeneous glass, we chose synthetic albite ($\text{NaAlSi}_3\text{O}_8$) as flux agent because it yields intermediate chemical compositions, which can melt at ~ 1450 °C (He *et al.* 2016). To minimise the effects of volatilisation, contamination and metal segregation during melting in temperature-controlled furnace at 1 atm, we apply the molybdenum–graphite assembly method of He *et al.* (2016). A preparation procedure to produce homogeneous glasses for peridotites is described, and precision and accuracy of trace element analyses are evaluated. The sample preparation and analyses were done at the University of Science and Technology of China (USTC).

Methods

Reference materials, samples and flux agent

Reference materials: Two USGS peridotite reference materials (PCC-1 and DTS-2B) were chosen for melting experiments to explore optimal conditions of melting. PCC-1 is composed of olivine (58%), orthopyroxene (9%) and serpentine (32%) (Table 1, Flanagan 1967). Minor minerals include primary disseminated chromite, secondary magnetite and traces of secondary talc and carbonate (Flanagan 1967). Mineralogical analysis of DTS-2B provided by USGS reveals that the dominant mineral is forsterite (> 90%) with minor amounts of chromite and trace amounts of lizardite (Table 1). Both reference materials have $\sim 40\%$ *m/m* SiO_2 and Mg\# ($100 \times \text{Mg}^{2+}/(\text{Mg}^{2+} + \text{Fe}^{2+})$) of ~ 92 . They represent the most refractory natural peridotites extremely low in incompatible elements.

Table 1.
The lithology, location and mineral compositions of two USGS peridotite reference materials (PCC-1 and DTS-2B) and three natural peridotite samples

| Sample name | USGS reference material | | Natural peridotite xenoliths | | |
|---------------------|--|---|---|--|--|
| | PCC-1 | DTS-2B | 16BY-01 | 15PSS-03 | 15TS-03 |
| Lithology | Harzburgite | Dunite | Lherzolite | Lherzolite | Lherzolite |
| Location | Sonoma Country, California, America | Twin Sisters, Washington, America | Beiyuan, Shandong, China | Panshishan, Jiangsu, China | Tashan, Jiangsu, China |
| Mineral composition | Olivine (58%), orthopyroxene (9%), serpentine (32%) with minor amounts of chromite and magnetite | Forsterite (> 90%) with minor amounts of chromite and trace amounts of lizardite | Olivine (70%), clinopyroxene (25%), orthopyroxene (3%) and spinel (2%) | Olivine (50%), orthopyroxene (30%), clinopyroxene (19%) and spinel (1%) | Olivine (70%), orthopyroxene (15%), clinopyroxene (14%) and spinel (1%) |

Natural samples: Three spinel lherzolite xenoliths (16BY-01, 15TS-03 and 15PSS-03) from Cenozoic alkali basalts in eastern China (Xiao *et al.* 2010, Zeng *et al.* 2013) were analysed using both the new method in this study and conventional solution ICP-MS for comparison. The xenoliths consist of olivine, orthopyroxene and clinopyroxene, as well as accessory (1–2%) Cr-Al spinel, and have SiO₂ content of ~ 45% *m/m* and Mg# of ~ 88. Their modal compositions determined by point counting in thin sections are provided in Table 1.

Flux agent: Considering the high liquidus temperatures of peridotites (Carswell 1968, Herzberg 1983), in order to make homogeneous melts in one-atmosphere furnace, it is necessary to add flux agent to promote the fusion. We use albite as flux agent because albite–peridotite mixtures melt rapidly at 1450 °C with the Mo capsule–graphite assembly and can be quenched to homogeneous glass (He *et al.* 2016). It is important to find appropriate sample-to-flux ratio (SFR) because more flux may increase contamination (Meisel *et al.* 2002, Eggins 2003) while less flux may not produce homogeneous glass.

The synthetic albite flux was prepared from pure (99.99%, Aladdin) Na₂CO₃, Al₂O₃ and SiO₂ at 1:1:2 molar ratios. The mixture was ground in an agate mortar under ethanol for 1 h and then decarbonated by heating to 1000 °C at 100 °C h⁻¹ and staying at 1000 °C for 48 h. After that, the mixture was ground again and melted at 1300 °C in a platinum crucible for 2 h. The melt was quenched to room temperature in air, and the glass was ground to 200 mesh powder.

High-temperature experiments

To determine the optimal fusion conditions, mixtures of powdered peridotite (PCC-1 or DTS-2B) and albite with a given ratio were weighed (total mass ~ 0.3 g) and put into a

Mo capsule–graphite assembly permitting to melt silicate rocks with SiO₂ ranging from 47 to 73% *m/m* efficiently (He *et al.* 2016). Experiments were conducted at the Experimental Petrology Lab in USTC in a high-temperature one-atmosphere furnace (KSL-1700X-A4, Hefei Kejing Material Technology Company, Hefei, China) with an intelligent programmable system to control the heating procedure. After heating, the melts were quenched by dropping the assembly into water.

Once the optimal fusion conditions were determined, we also conducted the following experiments at these conditions: (a) three runs with albite powders to detect the contamination effects from the flux; (b) repeated runs with PCC-1 (A13, A14) and DTS-2B (B13, B14) to investigate the reproducibility and repeatability of the method; and (c) runs with natural peridotite powders to verify the applicability of the new method. All experimental conditions are listed in Table 3. Random fragments of quenched materials were mounted in epoxy and polished for observation under electron microscope and LA-ICP-MS analyses. Aliquots of quenched materials were ground for powder X-ray diffraction (XRD) analyses.

Analytical methods

SEM and XRD: Textures of quenched materials were examined by back-scattered electron (BSE) imaging using the TESCAN MIRA 3 LMH field emission scanning electron microscopy (FE-SEM) at the USTC. The samples were coated with platinum (1.5 nm thick). The BSE images were obtained at 15 kV acceleration voltage and 20 nA beam current.

X-ray diffraction was used to look for quenched or residual minerals. The XRD patterns were recorded with a Japan Rigaku TTR-III X-ray Instrument equipped with graphite-monochromatised Cu K α irradiation ($\lambda = 0.154056$ nm) at the USTC employing a scanning rate of 0.02° per second in the 2 θ range 10–70°.

LA-ICP-MS: Trace element mass fractions were measured with an Agilent 7700e ICP-MS in combination with a GeoLasPro ArF (193 nm) excimer laser ablation system at the Chinese Academy of Sciences Key Laboratory of Crust-Mantle Materials and Environments, USTC. Helium was used as carrier gas during ablation, and argon was mixed with helium before entering the plasma. The carrier and make-up gas flows were optimised by ablating NIST SRM 610 to obtain maximum ^{208}Pb signal intensities while keeping ThO/Th (1.5–2%) and $\text{Ca}^{2+}/\text{Ca}^{+}$ (~0.2%) low enough to reduce the oxide and doubly charged ion interferences (Günther and Hattendorf 2005, Liu *et al.* 2008). As an indicator of complete vaporisation, the $^{238}\text{U}^{+}/^{232}\text{Th}^{+}$ was kept close to 1 when ablating NIST SRM 610 (Günther and Hattendorf 2005, Liu *et al.* 2008). Samples were ablated in single-spot mode, with a spot size of 44 μm and repetition rate of 10 Hz. Each spot analysis measurement consisted of an ~20 s background acquisition in time-resolved analysis mode, followed by the ablation of 40 s and gas flow washing of 35 s. NIST SRM 610 was repeatedly analysed after eight sample measurements for drift correction.

For data calibration, the *MRM-NoIS* approach (calibrated against multiple silicate reference materials without using an internal standard) was used as described in Liu *et al.* (2008) and Chen *et al.* (2011). For a given anhydrous silicate glass, the sum of mass fractions of all elements expressed as oxides (according to their oxidation states in the silicates) should be 100% *m/m*. Therefore, the mass fractions of elements can be determined by the following equations

$$C_{\text{sam}}^i = \frac{100 \times \text{cps}_{\text{sam}}^i \times I^i}{\sum_{k=1}^N (\text{cps}_{\text{sam}}^k \times I^k)} \quad (1)$$

$$I^i = \sum_{j=1}^n \left(\frac{C_{\text{mi}}^i}{\text{cps}_{\text{mi}}^i} \times \frac{C_{\text{mi}}^i}{\sum_{i=1}^n C_{\text{mi}}^i} \right) \quad (2)$$

where N is the number of elements that can be determined by LA-ICP-MS. Importantly, all major elements in the matrix need to be measured. C_{sam}^i is the mass fraction of analyte element i in the sample, C_{mi}^i is the mass fraction of analyte element i in the reference material j for calibration, $\text{cps}_{\text{sam}}^i$ ($\text{cps}_{\text{sam}}^k$) is the net count rate (sample signal minus background) of i (k) in the sample, cps_{mi}^i is the net count rate of i in the reference material j for calibration, and n is the number of reference materials used as calibrators. When multiple reference materials were used for calibration, I value can be calculated with regression statistics derived from the analysis of several reference materials.

In this study, three USGS basaltic glasses (BHVO-2G, BCR-2G and BIR-1G) were used as calibration reference materials. We also used two basaltic reference materials GSD-1G and TB-1G as secondary RMs (Table S1). Operating conditions and the isotopes collected using LA-ICP-MS are listed in Table 2. The detector modes listed in Table 2 were only used for the measurements of peridotite reference materials (PCC-1 and DTS-2B) and peridotite samples (16BY-01, 15TS-03 and 15PSS-03). For blanks, flux blanks, NIST SRM 610, three basaltic reference materials (BHVO-2G, BIR-1G and BCR-2G) and basaltic secondary RMs (GSD-1G and TB-1G), the detector modes used for all measured elements were pulse counting. Offline selection of signal interval of blank and sample measured, integration of background and ablation signals, time-drift correction and quantitative calibration were performed with ICPMSDataCal software (Liu *et al.* 2008).

Barium oxides can cause interference on Eu during LA-ICP-MS measurements (Kent and Ungerer 2005), with $^{135}\text{Ba}^{16}\text{O}/^{135}\text{Ba}$ of 0.04% at ThO⁺/Th⁺ at 2.5%. We estimate that $^{135}\text{Ba}^{16}\text{O}/^{135}\text{Ba}$ ranges from 0.024% to 0.032%, given that the ThO⁺/Th⁺ in our experiments is 1.5–2%. Therefore, the

Table 2.
Operation conditions for LA-ICP-MS and solution ICP-MS analyses

| ICP-MS conditions | LA-ICP-MS analysis | Solution ICP-MS analysis |
|-----------------------|---|---|
| ICP-MS instrument | Agilent 7700e | PerkinElmer Elan DRCII |
| RF Power | 1350 W | 1350 W |
| Nebuliser gas | | 1.1 l min ⁻¹ Ar |
| Plasma gas | 14 l min ⁻¹ Ar | 15 l min ⁻¹ Ar |
| Auxiliary gas | 0.9 l min ⁻¹ Ar | 1.15 l min ⁻¹ Ar |
| Make-up gas | 0.75 l min ⁻¹ Ar | |
| Isotopes ^a | ^{45}Sc , ^{48}Ti , ^{51}V , ^{53}Cr , ^{55}Mn , ^{59}Co , ^{60}Ni , ^{63}Cu , ^{66}Zn , ^{71}Ga , ^{85}Rb , ^{88}Sr , ^{89}Y , ^{91}Zr , ^{93}Nb , ^{137}Ba , ^{139}La , ^{140}Ce , ^{141}Pr , ^{143}Nd , ^{147}Sm , ^{151}Eu , ^{155}Gd , ^{159}Tb , ^{163}Dy , ^{165}Ho , ^{166}Er , ^{169}Tm , ^{173}Yb , ^{175}Lu , ^{178}Hf , ^{181}Ta , ^{208}Pb , ^{232}Th , ^{238}U | |
| Dwell time | 5 ms | 20 ms |
| Detector ^b | Dual (analogue counting for ^{53}Cr , pulse counting for all other elements) | Dual (analogue counting for ^{53}Cr , ^{55}Mn and ^{60}Ni , pulse counting for all other elements) |
| Laser system | GeoLasPro | |
| Wavelength | 193 nm | |
| Energy density | 10 J cm ⁻² | |
| Carrier gas | 0.9 l min ⁻¹ He | |
| Ablation style | Single spot | |
| Ablation spot size | 44 μm | |
| Repetition rate | 10 Hz | |

^a All of the isotopes listed were measured by both LA-ICP-MS and solution ICP-MS. ^b The detector modes were only conducted for the analysis of peridotite reference materials (PCC-1 and DTS-2B) and samples (16BY-01, 15PSS-01 and 15TS-03).

Table 3.
The experiment conditions and results (BSE and XRD)

| Sample | No. | SFR ^a | T (°C) | Duration (min) | BSE | XRD |
|----------|-----|------------------|--------|----------------|-------------------|--------------|
| PCC-1 | A01 | 1:1 | 1500 | 30 | Olivine, spinel | Forsterite |
| | A02 | 1:1 | 1550 | 30 | Olivine, spinel | Forsterite |
| | A03 | 1:1.5 | 1500 | 30 | Olivine | Forsterite |
| | A04 | 1:1.5 | 1550 | 30 | No minerals | Forsterite |
| | A05 | 1:2 | 1450 | 10 | No minerals | Amorphous |
| | A06 | 1:2 | 1500 | 5 | No minerals | Amorphous |
| | A07 | 1:2 | 1500 | 10 | No minerals | Amorphous |
| | A10 | 1:2 | 1500 | 15 | No minerals | Not examined |
| | A11 | 1:2 | 1500 | 20 | No minerals | Not examined |
| | A08 | 1:2 | 1500 | 30 | Small metal balls | Amorphous |
| | A09 | 1:2 | 1550 | 10 | No minerals | Amorphous |
| | A12 | 1:2 | 1550 | 15 | No minerals | Not examined |
| | A13 | 1:2 | 1500 | 10 | No minerals | Not examined |
| | A14 | 1:2 | 1500 | 10 | No minerals | Not examined |
| DTS-2B | B01 | 1:1 | 1500 | 30 | Olivine, spinel | Forsterite |
| | B02 | 1:1 | 1550 | 30 | Olivine, spinel | Forsterite |
| | B03 | 1:1.5 | 1500 | 30 | Olivine, spinel | Forsterite |
| | B04 | 1:1.5 | 1550 | 30 | No minerals | Forsterite |
| | B05 | 1:2 | 1450 | 10 | No minerals | Amorphous |
| | B06 | 1:2 | 1500 | 5 | No minerals | Amorphous |
| | B07 | 1:2 | 1500 | 10 | No minerals | Amorphous |
| | B10 | 1:2 | 1500 | 15 | No minerals | Not examined |
| | B11 | 1:2 | 1500 | 20 | No minerals | Not examined |
| | B08 | 1:2 | 1500 | 30 | Small metal balls | Amorphous |
| | B09 | 1:2 | 1550 | 10 | No minerals | Amorphous |
| | B12 | 1:2 | 1550 | 15 | No minerals | Not examined |
| | B13 | 1:2 | 1500 | 10 | No minerals | Not examined |
| | B14 | 1:2 | 1500 | 10 | No minerals | Not examined |
| 16BY-01 | C01 | 1:2 | 1500 | 10 | No minerals | Not examined |
| 15PSS-03 | C02 | 1:2 | 1500 | 10 | No minerals | Not examined |
| 15TS-03 | C03 | 1:2 | 1500 | 10 | No minerals | Not examined |
| Blank-1 | D01 | – | 1500 | 10 | No minerals | Not examined |
| Blank-2 | D02 | – | 1500 | 10 | No minerals | Not examined |
| Blank-3 | D03 | – | 1500 | 10 | No minerals | Not examined |

^a SFR – sample-to-flux ratio.

Ba oxide interferences on ¹⁵¹Eu were corrected in this study using the equation $^{151}\text{Eu}_{\text{corrected}} = ^{151}\text{Eu}_{\text{measured}} - 0.00028 \times ^{135}\text{Ba}$, assuming that the $^{135}\text{Ba}/^{135}\text{Ba}^{16}\text{O}/^{135}\text{Ba}$ is 0.028%.

Solution ICP-MS: Two reference materials (PCC-1 and DTS-2B) and three peridotite samples (16BY-01, 15TS-03 and 15PSS-03) from eastern China containing 1–2% of Cr-Al spinel were analysed by solution ICP-MS to evaluate the accuracy of our new method. The digestion procedure in HNO₃-HF mixture was that of Hou and Wang (2007) except that its duration was extended to 5 days to favour spinel dissolution.

Trace element mass fraction data were acquired using a PerkinElmer Elan DRCII ICP-MS. The auto lens voltages and nebuliser gas flow rate were optimised using the solution of 5 ng ml⁻¹ ⁹Be, ⁵⁹Co, ¹¹⁵In, ¹⁵⁹Tb and ²⁰⁹Bi (2% HNO₃).

Multi-element mixed external standard solutions were prepared from 1.0 mg ml⁻¹ of single-element standard solutions (Spex CertiPrep) and listed in Table S2. Drift corrections were performed by using Rh as an internal standard and by repeatedly analysing an 'external' standard solution (std-2, Table S2) every eight sample measurements. Reference materials BHVO-2 and BCR-2, digested using the same method as that described above, were used as secondary RMs during ICP-MS analysis. Table 2 lists the operating conditions and the isotopes measured with solution ICP-MS. Note that the detector modes listed in Table 2 were only used for the measurements of peridotites (PCC-1, DTS-2B, 16BY-01, 15TS-03 and 15PSS-03). For blanks, multi-element mixed external standard solutions and secondary RMs (BHVO-2 and BIR-1), the detector mode was pulse counting for all elements. The ICP-MS data were also reduced using ICPMSDataCal software (Liu *et al.* 2008).

Results and discussion

Optimal fusion conditions

Optimising fusion conditions (sample-to-flux ratio, temperature and duration) is critical to efficiently obtain homogeneous glasses for analyses. Importantly, melting procedure should minimise the loss of volatile elements (e.g., Zn and Pb; Stoll *et al.* 2008, Reading *et al.* 2017) and migration of transition elements (e.g., Ni and Cr) into capsules (Kurosawa *et al.* 2006, He *et al.* 2016).

The experiments with PCC-1 and DTS-2B were performed with variable sample-to-flux ratio (SFR), temperature and duration (Table 3). Our major objective was to obtain homogeneous glass. BSE images and XRD data showed residues of olivine and/or spinel in the quenched glasses at 1550 °C, fusion duration of 30 min and SFR of 1:1 or 1:1.5 (Table 3, Figures 1a, b and 2b). However, no residual refractory minerals in the quenched glasses were observed when the SFR was reduced to 1:2 in the temperature range from 1450 to 1550 °C and fusion duration from 10 to 20 min (Table 3, Figures 1d and 2a). On the other hand, when the fusion duration was extended to 30 min at 1500 °C, small metal balls were observed in quenched glass (Figure 1c). We infer that homogeneous quenched glass can best be obtained with the SFR of 1:2 with the heating duration of no more than 20 min.

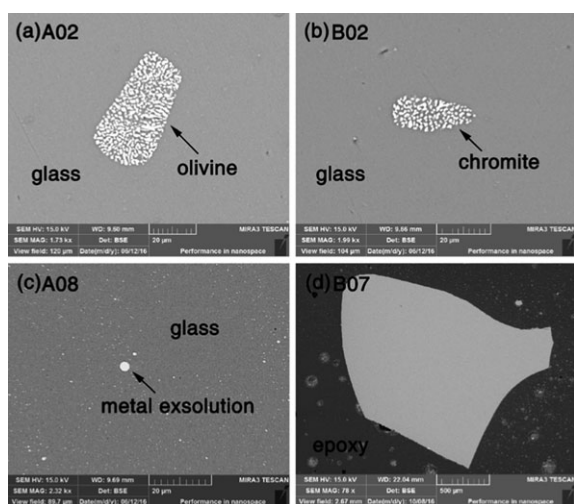


Figure 1. Back-scattered electron images of quenched glasses synthesised at different experimental conditions. (a–b) Melting of PCC-1 (a) and DTS-2B (b) at 1550 °C for 30 min with SFR of 1:1; (c–d) melting of PCC-1 (c) for 30 min and DTS-2B (d) for 10 min at 1500 °C with SFR of 1:2.

Several elements were chosen to explore the effects of volatilisation, contamination and the persistence of refractory mineral residues. Previous studies suggested that volatile elements (Zn and Pb) and siderophile elements (Ni) were sensitive to the temperature and duration of fusion (Stoll *et al.* 2008, Regnery *et al.* 2010, Bao *et al.* 2016). Because the partition coefficient of Ni between olivine and mafic melts is very high (e.g., Herzberg *et al.* 2013), Ni mass fraction in the glass can be used to monitor olivine preservation or precipitation during fusion and/or quenching. Cr-Al spinel is a major host of Cr in spinel and garnet-spinel facies peridotites (e.g., Bodinier and Godard 2014, Pearson *et al.* 2014). Partition coefficients of chromium and vanadium between spinel and liquid are very high (Canil 2002, Klemme *et al.* 2006), suggesting that these elements should be concentrated in spinel if this mineral is present in quenched glasses. This is why Cr and V mass fractions in glass are used to monitor the presence of spinel.

To test the accuracy and precision of our method, element mass fractions in PCC-1 and DTS-2B obtained in this study are normalised to reference values from Govindaraju (1994) and USGS certification, respectively, as follows:

$$F^N = C^M / C^R \quad (3)$$

where F^N , C^M and C^R are the normalised factor, the average measured and the reference mass fractions from the literature, respectively.

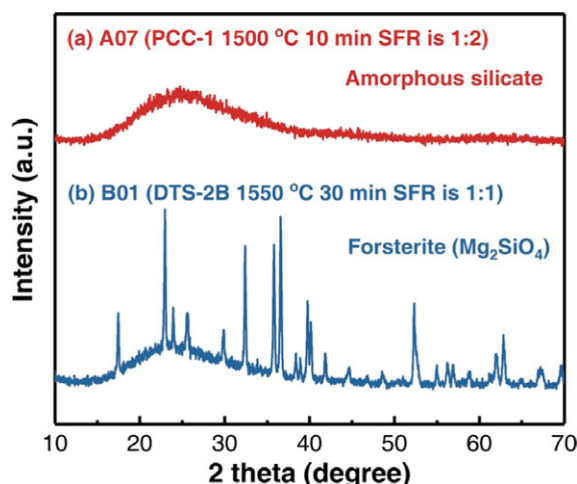


Figure 2. XRD patterns of quenched glasses at different melting experimental conditions. (a) Amorphous silicate; (b) amorphous silicate containing forsterite.

Figure 3 shows that the normalised Cr, V, Ni, Zn and Pb factors vary with the duration of experiments at 1500 °C and SFR of 1:2. Some experiments (A13, A14 and B13, B14 for A7 and B7, respectively) are not included in Figures 3 and 4 or Table 4 for this section, because they were conducted after the optimal fusion conditions were determined. Normalised Cr, V and Ni factors in quenched glasses of PCC-1 and DTS-2B are below 0.9 for a short fusion duration of 5 min, indicating the presence of residual spinel and olivine (Figure 3 and Table 4). By comparison, at fusion periods longer than 20 min, great discrepancies were observed for normalised Ni, Pb and Zn factors in fused glasses of both PCC-1 and DTS-2B (Figure 3 and Table 4), suggesting losses of these elements. The loss of Ni may be attributed to the reaction between the silicate melt and Mo capsule, which produced small metal globules (Figure 1c) in

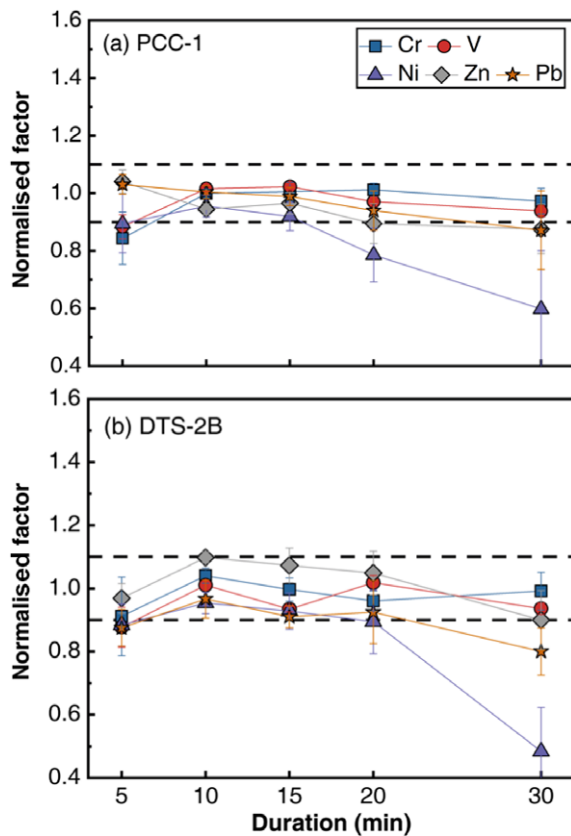


Figure 3. Normalised Cr, V, Ni, Zn and Pb factors of quenched glasses measured with LA-ICP-MS for (a) PCC-1 and (b) DTS-2B as a function of duration for experiments at 1500 °C and SFR of 1:2. The Cr, V, Zn, Pb and Ni reference mass fractions of PCC-1 and DTS-2B for calculating normalised factors are from Govindaraju (1994) and the USGS certificate, respectively. Data are reported in Table 4.

quenched glasses, while the loss of Zn and Pb can be attributed to volatilisation (Stoll *et al.* 2008). Altogether, this suggests that fusion periods of 20 min or longer at 1500 °C may lead to depletions of volatile and highly siderophile elements in the melt. We conclude that moderate fusion duration (10–15 min) at 1500 °C with the SRF of 1:2 yields the best results.

Figure 4 illustrates temperature effects on normalised Cr, V, Ni, Zn and Pb factors (F_{Element}^N) of quenched glasses of PCC-1 and DTS-2B at 10 min fusion duration and the SFR of 1:2. F_{Cr}^N , F_{V}^N and F_{Ni}^N for DTS-2B, and F_{Cr}^N for PCC-1 are lower than 0.9 at 1450 °C, indicating olivine and spinel may not completely melt at 1450 °C. For experiments performed at 1500 and 1550 °C, Cr, V, Ni, Zn and Pb mass fractions of quenched glasses are consistent with literature values (Figure 4). Therefore, temperature ranging from 1500–

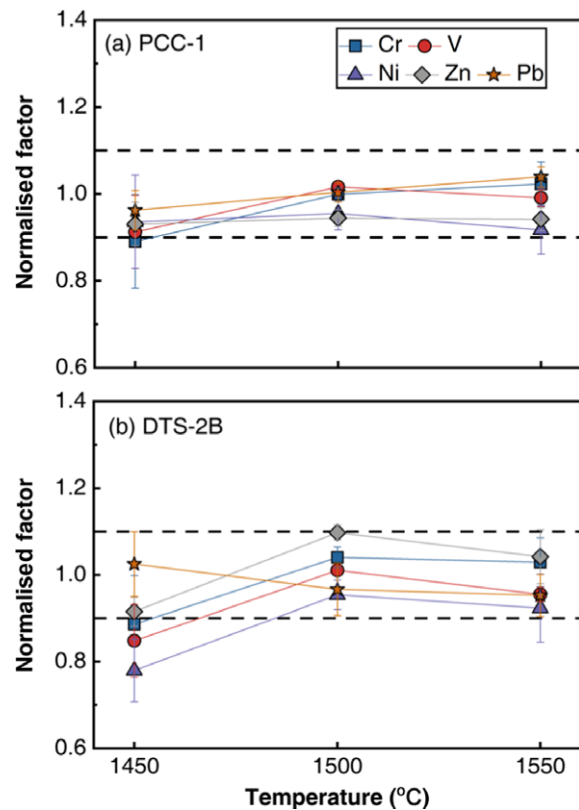


Figure 4. Normalised Cr, V, Ni, Zn and Pb factors of quenched glasses for (a) PCC-1 and (b) DTS-2B as a function of temperature at melting interval of 10 min and SFR of 1:2. The Cr, V, Zn, Pb and Ni reference mass fractions of PCC-1 and DTS-2B for calculating normalised factors are from Govindaraju (1994) and the USGS certificate, respectively. Data are reported in Table 4.

Table 4.
Chromium, V, Zn, Pb and Ni mass fractions obtained from experiments to determine the optimal fusion conditions

| Sample | No. | Element mass fraction ($\mu\text{g g}^{-1}$) | | | | | | | | | | |
|--------|-----|--|--------------|-------------------------|------------|-------------------------|------------|-------------------------|------------|-------------------------|-----------|-------------------------|
| | | n^a | Cr | Normalised ^b | V | Normalised ^b | Ni | Normalised ^b | Zn | Normalised ^b | Pb | Normalised ^b |
| PCC-1 | A05 | 9 | 2432 (294) | 0.89 | 28.3 (2.6) | 0.91 | 2228 (256) | 0.94 | 39.1 (2.1) | 0.93 | 8.5 (0.4) | 0.96 |
| | A06 | 8 | 2304 (248) | 0.84 | 27.4 (1.3) | 0.88 | 2132 (243) | 0.90 | 43.7 (1.7) | 1.04 | 9.1 (0.3) | 1.03 |
| | A07 | 12 | 2728 (40) | 1.00 | 31.5 (0.3) | 1.02 | 2273 (89) | 0.96 | 39.7 (0.8) | 0.94 | 8.8 (0.2) | 1.00 |
| | A10 | 10 | 2745 (88) | 1.01 | 31.7 (0.3) | 1.02 | 2189 (116) | 0.92 | 40.6 (1.6) | 0.97 | 8.7 (0.3) | 0.99 |
| | A11 | 11 | 2762 (62) | 1.01 | 30.1 (0.5) | 0.97 | 1872 (223) | 0.79 | 37.6 (2.9) | 0.90 | 8.3 (0.6) | 0.94 |
| | A08 | 8 | 2656 (121) | 0.97 | 29.1 (0.6) | 0.94 | 1423 (482) | 0.60 | 36.8 (3.6) | 0.88 | 7.7 (1.2) | 0.87 |
| | A09 | 15 | 2793 (139) | 1.02 | 30.7 (0.6) | 0.99 | 2184 (133) | 0.92 | 39.6 (1.1) | 0.94 | 9.2 (0.2) | 1.04 |
| | A12 | 14 | 2648 (83) | 0.97 | 31.2 (0.6) | 1.01 | 2203 (104) | 0.93 | 41.5 (2.9) | 0.99 | 8.8 (0.7) | 1.00 |
| | B05 | 7 | 13742 (1734) | 0.89 | 18.5 (1.7) | 0.84 | 2948 (273) | 0.78 | 41.2 (1.5) | 0.92 | 4.1 (0.3) | 1.03 |
| | B06 | 5 | 14130 (1934) | 0.91 | 19.3 (1.4) | 0.88 | 3342 (253) | 0.88 | 43.6 (2.1) | 0.97 | 3.5 (0.2) | 0.88 |
| | B07 | 8 | 16130 (368) | 1.04 | 22.2 (0.2) | 1.01 | 3607 (128) | 0.95 | 49.4 (0.8) | 1.10 | 3.9 (0.2) | 0.97 |
| B10 | 10 | 15454 (570) | 1.00 | 20.5 (0.2) | 0.93 | 3508 (217) | 0.93 | 48.3 (2.5) | 1.07 | 3.6 (0.1) | 0.91 | |
| B11 | 12 | 14892 (483) | 0.96 | 22.4 (0.5) | 1.02 | 3382 (382) | 0.89 | 47.2 (3.1) | 1.05 | 3.7 (0.4) | 0.93 | |
| B08 | 10 | 15372 (927) | 0.99 | 20.6 (0.4) | 0.94 | 1830 (523) | 0.48 | 40.5 (4.2) | 0.90 | 3.2 (0.3) | 0.80 | |
| B09 | 6 | 15954 (874) | 1.03 | 21.1 (0.4) | 0.96 | 3491 (296) | 0.92 | 46.9 (2.8) | 1.04 | 3.8 (0.2) | 0.95 | |
| B12 | 8 | 16133 (734) | 1.04 | 21.8 (0.7) | 0.99 | 3528 (241) | 0.93 | 48.6 (3.1) | 1.08 | 4.2 (0.3) | 1.05 | |

Numbers in brackets are one standard deviation on the average of multiple analyses.

^a n represents for the numbers of analyses.

^b The reference mass fractions of PCC-1 and DTS-2B for calculation of normalised mass fractions are from Govindaraju (1994) and the USGS certificate, respectively.

Table 5.
Instrumental detection limits, three blanks, flux blank and GeoReM compiled PCC-1 trace element values from Govindaraju (1994)

| Element | Detection limits ($\mu\text{g g}^{-1}$) | Blank 1 ($n = 15, \mu\text{g g}^{-1}$) | Blank 2 ($n = 20, \mu\text{g g}^{-1}$) | Blank 3 ($n = 12, \mu\text{g g}^{-1}$) | Flux blank ($n = 47, \mu\text{g g}^{-1}$) | PCC-1 ($\mu\text{g g}^{-1}$) |
|---------|--|---|---|---|--|-----------------------------------|
| Sc | 0.13 | < DL | < DL | < DL | < DL | 8.4 |
| Ti | 0.09 | 0.62 (0.03) | 0.59 (0.02) | 0.61 (0.04) | 0.60 (0.04) | 75 |
| V | 0.09 | < DL | < DL | < DL | < DL | 31 |
| Cr | 0.74 | < DL | < DL | < DL | < DL | 2730 |
| Mn | 0.67 | < DL | < DL | < DL | < DL | 929.3 |
| Co | 0.04 | 0.08 (0.02) | 0.08 (0.01) | 0.08 (0.02) | 0.08 (0.02) | 112 |
| Ni | 1.01 | 1.23 | 1.23 | 1.23 | 1.23 | 2380 |
| Cu | 0.54 | < DL | < DL | < DL | < DL | 10 |
| Zn | 0.20 | < DL | < DL | < DL | < DL | 42 |
| Ga | 0.02 | 0.037 (0.008) | 0.033 (0.006) | 0.036 (0.010) | 0.035 (0.008) | 0.7 |
| Rb | 0.01 | 0.014 (0.005) | 0.012 (0.003) | 0.014 (0.002) | 0.013 (0.004) | 0.066 |
| Sr | 0.04 | < DL | < DL | < DL | < DL | 0.4 |
| Y | 0.006 | < DL | < DL | < DL | < DL | 0.1 |
| Zr | 0.08 | < DL | < DL | < DL | < DL | 10 |
| Nb | 0.007 | < DL | < DL | < DL | < DL | 1 |
| Ba | 0.02 | 0.058 (0.008) | 0.062 (0.006) | 0.058 (0.005) | 0.060 (0.007) | 1.2 |
| La | 0.002 | 0.004 (0.001) | 0.004 (0.001) | 0.005 (0.001) | 0.004 (0.001) | 0.052 |
| Ce | 0.004 | < DL | < DL | < DL | < DL | 0.1 |
| Pr | 0.0025 | < DL | < DL | < DL | < DL | 0.013 |
| Nd | 0.011 | < DL | < DL | < DL | < DL | 0.042 |
| Sm | 0.003 | < DL | < DL | < DL | < DL | 0.0066 |
| Eu | 0.002 | < DL | < DL | < DL | < DL | 0.0018 |
| Gd | 0.006 | < DL | < DL | < DL | < DL | 0.014 |
| Tb | 0.001 | < DL | < DL | < DL | < DL | 0.0015 |
| Dy | 0.01 | < DL | < DL | < DL | < DL | 0.01 |
| Ho | 0.002 | < DL | < DL | < DL | < DL | 0.0025 |
| Er | 0.006 | < DL | < DL | < DL | < DL | 0.012 |
| Tm | 0.002 | < DL | < DL | < DL | < DL | 0.0027 |
| Yb | 0.01 | < DL | < DL | < DL | < DL | 0.024 |
| Lu | 0.001 | < DL | < DL | < DL | < DL | 0.0057 |
| Hf | 0.005 | < DL | < DL | < DL | < DL | 0.04 |
| Ta | 0.01 | < DL | < DL | < DL | < DL | 0.02 |
| Pb | 0.03 | 0.035 (0.009) | 0.035 (0.007) | 0.033 (0.010) | 0.034 (0.009) | 10 |
| Th | 0.003 | < DL | < DL | < DL | < DL | 0.013 |
| U | 0.003 | < DL | < DL | < DL | < DL | 0.0045 |

Numbers in brackets are one standard deviation of the mean of multiple analyses. n is the number of analyses averaged.

1550 °C should be appropriate for melting with 10 min duration and SFR of 1:2.

In summary, for peridotite, we adopted a temperature range from 1500 to 1550 °C, fusion duration from 10 to 15 min and SFR of 1:2 as the optimal operating conditions for making homogeneous glass. For simplifying the fusing procedure, we performed the rest of the experiments at 1500 °C for 10 min with SFR of 1:2.

Detection limits and flux blank

With the sample-to-flux ratio (SFR) of 1:2, the detection limits should reflect a threefold dilution of sample in the fused beads. The detection limits are listed in Table 5 in compar-

ison with reference values (Govindaraju 1994). Following Longerich *et al.* (1996) and Liu *et al.* (2008), the limit of detection (LOD) for an element (i) can be estimated as follows:

$$\text{LOD}^i = 3 \times (3 \times \sigma_{\text{Bgd}} / \sqrt{n}) \times \sqrt{2} / S \quad (4)$$

$$\left(S = \frac{\sum_{i=1}^N (\text{cps}_{\text{sam}}^i \times I^i)}{100 \times I^i} \right)$$

where σ_{Bgd} and n are the standard deviation and number of determinations of the background, respectively. Calculated detection limits based on measured background count rates and sensitivities during analysis of the NIST SRM 610 glass are listed in Table 5.

The first series transition element (Sc, Ti, V, Cr, Mn, Co, Ni, Cu and Zn) mass fractions in PCC-1 are about two orders of magnitude higher than their detection limits ($\sim 10^{-1}$ to $\sim 10^{-2}$ $\mu\text{g g}^{-1}$), indicating that transition elements can be measured accurately with our method even in the most refractory, melt-depleted peridotites (Table 5). However, the contents of the REE, Th and U in PCC-1 are similar to the detection limits ($\sim 10^{-3}$ $\mu\text{g g}^{-1}$), suggesting that obtaining accurate mass fractions may be challenging (Table 5).

Impurities in albite flux may affect the accuracy of the measurements as well. To investigate the contamination effects, three flux blanks were prepared by fusing albite powders at the same melting conditions as for peridotite. Results for each blank contain the analyses of random fragments of quenched glasses in one experiment. The results of the three blanks are consistent (Table 5). An average of all three blanks was used as the flux blank for our data reduction.

The flux blank contains small but significant amounts of several elements which, after taking into account the threefold sample dilution, contribute the following share of their mass fractions in PCC-1: 0.07% Co, 0.80% Ti, 0.05% Ni, 5.00% Ga, 19.6% Rb, 5.00% Ba, 7.69% La and 0.34% Pb. These elemental blanks contribute significantly to the mass fractions of Ga, Rb, Ba and La (Table 5). Therefore, the measured Ga, Rb, Ba and La mass fractions were corrected by subtracting the contribution of the flux blank taking into account the threefold sample dilution.

Precision and accuracy of trace element determinations of reference materials and natural peridotites

Trace element mass fractions in two USGS reference materials (PCC-1 and DTS-2B) and three natural samples (16BY-01, 15PSS-03 and 15TS-03) were measured using the albite fusion method (Tables 6 and 7). Precision of the analyses can be expressed as standard deviation (1s, $\mu\text{g g}^{-1}$) and relative standard deviation (% RSD) values, while accuracy is judged by comparing results from different methods and published reference values.

To verify the reproducibility and repeatability of our study, we present the results of three randomly selected slices of glass in one experiment and repeated experiments on PCC-1 (A13, A14) and DTS-2B (B13, B14) at optimum conditions (Tables 3 and 6). Consistent trace elements mass fractions were obtained from random samples of the same experiments (A7 for PCC-1 and B7 for DTS-2B, Table 6). Meanwhile, repeated runs for PCC-1 and DTS-2B also show that the trace elements mass fractions were consistent within

uncertainties (Table 6). Those experiments and measurements demonstrate that the method developed has sufficient reproducibility and repeatability. For the discussion below, averaged trace elements mass fractions of all three experiments are used (Table 6).

Figure 5 shows that the RSD values of trace element mass fractions for PCC-1 and DTS-2B are generally lower than 10% for transition elements (Sc, Ti, V, Cr, Mn, Co, Ni, Cu and Zn), Ba and Pb, and $\sim 10\%$ for Zr, Rb and Sr, indicating that these elements can be measured precisely. However, REE, Y, Nb, HFSE (Hf, Ta), Th and U show relatively high RSD values ($> 10\%$), which may be attributed to the combination of high detection limits and low mass fractions in the peridotites (Table 6), in particular in the highly refractory peridotite PCC-1 and DTS-2B.

To assess accuracy, Figure 6 compares chondrite-normalised (McDonough and Sun 1995) trace element patterns obtained with the albite fusion method in this study with literature data for PCC-1 and DTS-2B, all of which are listed in Table 6 and Table S3 (Ionov *et al.* 1992, Govindaraju 1994, Eggins *et al.* 1997, Makishima *et al.* 2002, Eggins 2003, Qi *et al.* 2005, Makishima and Nakamura 2006, Robin-Popieul *et al.* 2012). Because Tm mass fraction data are not available for DTS-2B in the literature, and the trace element mass fractions in DTS-2B must be similar to those for DTS-2, we also compare our DTS-2B results with published DTS-2 data (Table 6 and Table S3) (Ila and Frey 2000, Raczek *et al.* 2001, Nakamura and Chang 2007, Ulrich *et al.* 2012). The mass fractions measured in this study are in good agreement with published results for transition elements (Sc, Ti, V, Cr, Mn, Co, Ni, Cu and Zn), LILE (Rb, Sr, Ba, Pb) and Zr. Note that the mass fractions of Ti and Zr in PCC-1 determined with the albite fusion method are lower than early data compiled in Govindaraju (1994), but are consistent with solution ICP-MS results in Ionov *et al.* (1992) and LA-ICP-MS results in Eggins (2003). Additionally, the Ga content ($0.48 \mu\text{g g}^{-1}$) in DTS-2B is lower than literature values ($0.93 \mu\text{g g}^{-1}$, Day *et al.* 2015; $0.94 \mu\text{g g}^{-1}$, Rospabé *et al.* 2018). For REE, Y, Nb and HFSE (Hf, Ta, Th and U), the results we obtained are not in good agreement with literature data (Figure 6, Table 6 and Table S3). This could be attributed to the very low mass fractions of these elements in PCC-1 and DTS-2B that are close to detection limits (Figure 5).

The reference materials (PCC-1 and DTS-2B) were also analysed for trace elements by the conventional acid digestion and solution ICP-MS method as in Hou and Wang (2007). The mass fractions obtained using the conventional method agree well with the literature ICP-MS data (Figure 6), indicating that the conventional acid digestion procedure used here

Table 6.
Trace element contents (in $\mu\text{g g}^{-1}$) in PCC-1 and DTS-2B from this study

| Element | PCC-1 | | | | | | | Solution ICP-MS |
|---------|-------------------|-------------------|-------------------|-----------------|-----------------|-----------------|-------|--------------------|
| | A07 | | | A13 | A14 | Mean, n = 58 | % RSD | |
| | LA-ICP-MS | | | n = 8 | n = 12 | n = 58 | | |
| | Slice 1 n = 12 | Slice 2 n = 16 | Slice 3 n = 10 | | | | | |
| Sc | 8.455 (0.181) | 8.550 (0.281) | 8.343 (0.081) | 8.571 (0.220) | 8.499 (0.286) | 8.487 (0.166) | 2 | 9.066 |
| Ti | 25.25 (0.49) | 25.43 (0.62) | 25.70 (0.36) | 24.86 (0.27) | 25.27 (0.380) | 25.32 (0.329) | 1 | 24.34 |
| V | 31.51 (0.31) | 31.69 (0.20) | 31.72 (0.35) | 32.73 (0.52) | 31.72 (0.41) | 31.81 (0.28) | 1 | 33.22 |
| Cr | 2728 (40) | 2673 (77) | 2745 (88) | 2638 (112) | 2749 (39) | 2708 (57) | 2 | 3152 |
| Mn | 922.2 (17.4) | 938.9 (16.7) | 931.2 (16.2) | 923.6 (27.3) | 919.7 (15.7) | 928.0 (14.3) | 2 | 931.3 |
| Co | 119.3 (1.1) | 118.8 (1.8) | 115.7 (1.5) | 117.2 (2.3) | 120.2 (0.8) | 118.4 (1.2) | 1 | 117.4 |
| Ni | 2273 (89) | 2356 (134) | 2277 (117) | 2309 (114) | 2384 (116) | 2324 (86) | 4 | 2261 |
| Cu | 9.013 (0.289) | 9.065 (0.305) | 8.823 (0.290) | 8.933 (0.308) | 9.104 (0.352) | 9.002 (0.231) | 3 | 8.704 |
| Zn | 39.68 (0.78) | 38.67 (1.69) | 40.55 (1.57) | 41.47 (1.92) | 39.57 (2.12) | 39.77 (1.25) | 3 | 45.73 |
| Ga | 0.623 (0.020) | 0.596 (0.502) | 0.620 (0.038) | 0.635 (0.044) | 0.607 (0.066) | 0.613 (0.035) | 6 | 0.596 |
| Rb | 0.061 (0.006) | 0.066 (0.014) | 0.060 (0.006) | 0.071 (0.008) | 0.060 (0.007) | 0.063 (0.006) | 10 | 0.090 |
| Sr | 0.360 (0.019) | 0.372 (0.011) | 0.377 (0.021) | 0.366 (0.014) | 0.389 (0.011) | 0.373 (0.012) | 3 | 0.336 |
| Y | 0.082 (0.007) | 0.080 (0.004) | 0.091 (0.007) | 0.083 (0.011) | 0.081 (0.011) | 0.083 (0.006) | 8 | 0.096 |
| Zr | 0.236 (0.014) | 0.243 (0.018) | 0.256 (0.020) | 0.221 (0.011) | 0.234 (0.012) | 0.239 (0.011) | 5 | 0.258 |
| Nb | 0.019 (0.002) | 0.017 (0.004) | 0.017 (0.003) | 0.015 (0.001) | 0.018 (0.002) | 0.017 (0.002) | 12 | 0.016 |
| Ba | 0.860 (0.044) | 0.852 (0.045) | 0.916 (0.053) | 0.883 (0.036) | 0.879 (0.060) | 0.875 (0.036) | 4 | 1.055 |
| La | 0.049 (0.003) | 0.048 (0.003) | 0.050 (0.011) | 0.048 (0.004) | 0.045 (0.004) | 0.048 (0.004) | 9 | 0.038 |
| Ce | 0.068 (0.007) | 0.062 (0.008) | 0.069 (0.008) | 0.067 (0.007) | 0.072 (0.009) | 0.067 (0.006) | 9 | 0.070 |
| Pr | 0.0083 (0.0015) | 0.0078 (0.0017) | 0.0082 (0.0013) | 0.0075 (0.0009) | 0.0083 (0.0013) | 0.0080 (0.0010) | 13 | 0.0091 |
| Nd | 0.027 (0.003) | 0.033 (0.005) | 0.025 (0.004) | 0.024 (0.002) | 0.028 (0.004) | 0.028 (0.003) | 10 | 0.038 |
| Sm | 0.0075 (0.0010) | 0.0074 (0.0010) | 0.0067 (0.0009) | 0.0071 (0.0007) | 0.0078 (0.0006) | 0.0073 (0.0006) | 9 | 0.0077 |
| Eu | 0.0027 (0.0005) | 0.0025 (0.0006) | 0.0031 (0.0005) | 0.0028 (0.0004) | 0.0027 (0.0003) | 0.0027 (0.0004) | 13 | 0.0020 |
| Gd | 0.0064 (0.0013) | 0.0072 (0.0008) | 0.0074 (0.0007) | 0.0078 (0.0013) | 0.0067 (0.0008) | 0.0071 (0.0008) | 11 | 0.0083 |
| Tb | 0.0021 (0.0006) | 0.0023 (0.008) | 0.0015 (0.0004) | 0.0025 (0.0005) | 0.0024 (0.0004) | 0.0022 (0.0004) | 19 | 0.0017 |
| Dy | 0.011 (0.002) | 0.012 (0.002) | 0.012 (0.001) | 0.012 (0.001) | 0.012 (0.001) | 0.012 (0.001) | 10 | 0.011 |
| Ho | 0.0026 (0.0008) | 0.0028 (0.005) | 0.0023 (0.0011) | 0.0024 (0.0009) | 0.0026 (0.0004) | 0.0026 (0.0006) | 23 | 0.0034 |
| Er | 0.016 (0.003) | 0.016 (0.004) | 0.014 (0.002) | 0.018 (0.002) | 0.011 (0.001) | 0.015 (0.002) | 13 | 0.013 |
| Tm | 0.0048 (0.0013) | 0.0040 (0.0008) | 0.0036 (0.0008) | 0.0052 (0.0011) | 0.0043 (0.0009) | 0.0043 (0.0007) | 17 | 0.0030 |
| Yb | 0.025 (0.004) | 0.024 (0.003) | 0.030 (0.004) | 0.024 (0.004) | 0.029 (0.006) | 0.026 (0.003) | 12 | 0.026 |
| Lu | 0.0047 (0.0010) | 0.0051 (0.0007) | 0.0052 (0.0007) | 0.0037 (0.0008) | 0.0042 (0.0007) | 0.0047 (0.0006) | 13 | 0.0061 |

Table 6 (continued).
Trace element contents (in $\mu\text{g g}^{-1}$) in PCC-1 and DTS-2B from this study

| Element | PCC-1 | | | | | | | | | | Solution ICP-MS | |
|----------------|-------------------|-------------------|-------------------|-------------------|-----------------|-----------------|-----------------|-----------------|-----------------|-----------------|----------------------------|--------|
| | LA-ICP-MS | | | | | | LA-ICP-MS | | | | | % RSD |
| | A07 | | | A13 | A14 | Mean, n = 58 | B13 | | | Mean, n = 46 | | |
| | Slice 1 n = 12 | Slice 2 n = 16 | Slice 3 n = 10 | n = 8 | n = 12 | | B13 | B14 | | | | |
| Hf | 0.0083 (0.0016) | 0.0096 (0.0009) | 0.0090 (0.0010) | 0.0098 (0.0014) | 0.0078 (0.0011) | 0.0089 (0.0009) | 0.0098 (0.0014) | 0.0078 (0.0011) | 0.0089 (0.0009) | 0.0089 (0.0009) | 11 | 0.0080 |
| Ta | 0.011 (0.002) | 0.013 (0.005) | 0.015 (0.004) | 0.010 (0.001) | 0.014 (0.004) | 0.0128 (0.0026) | 0.010 (0.001) | 0.014 (0.004) | 0.0128 (0.0026) | 0.0128 (0.0026) | 21 | 0.0034 |
| Pb | 8.866 (0.199) | 8.698 (0.216) | 8.902 (0.279) | 9.249 (0.324) | 9.179 (0.206) | 8.943 (0.186) | 9.249 (0.324) | 9.179 (0.206) | 8.943 (0.186) | 8.943 (0.186) | 2 | 9.593 |
| Th | 0.012 (0.002) | 0.014 (0.002) | 0.016 (0.003) | 0.010 (0.002) | 0.012 (0.003) | 0.013 (0.002) | 0.010 (0.002) | 0.012 (0.003) | 0.013 (0.002) | 0.013 (0.002) | 13 | 0.016 |
| U | 0.0056 (0.0011) | 0.0062 (0.0012) | 0.0054 (0.009) | 0.0049 (0.0013) | 0.0050 (0.0013) | 0.0055 (0.0009) | 0.0049 (0.0013) | 0.0050 (0.0013) | 0.0055 (0.0009) | 0.0055 (0.0009) | 16 | 0.0069 |
| Element | DTS-2B | | | | | | | | | | Solution ICP-MS | |
| | B07 | | | | | | LA-ICP-MS | | | | % RSD | |
| | Slice 2 n = 12 | | | Slice 3 n = 10 | | | B13 | B14 | Mean, n = 46 | | | |
| | Slice 1 n = 8 | Slice 2 n = 12 | Slice 3 n = 10 | n = 8 | n = 12 | n = 10 | n = 8 | n = 8 | | | | |
| Sc | 3.143 (0.140) | 3.109 (0.204) | 2.963 (0.194) | 3.135 (0.112) | 3.027 (0.132) | 3.073 (0.120) | 3.135 (0.112) | 3.027 (0.132) | 3.073 (0.120) | 3.073 (0.120) | 4 | 3.173 |
| Ti | 56.34 (3.76) | 58.48 (4.22) | 54.73 (2.23) | 52.19 (3.32) | 57.61 (1.63) | 56.05 (2.37) | 52.19 (3.32) | 57.61 (1.63) | 56.05 (2.37) | 56.05 (2.37) | 4 | 58.21 |
| V | 22.23 (0.25) | 21.72 (0.29) | 22.56 (0.19) | 22.55 (0.07) | 22.01 (0.16) | 22.19 (0.15) | 22.55 (0.07) | 22.01 (0.16) | 22.19 (0.15) | 22.19 (0.15) | 1 | 19.92 |
| Cr | 16130 (368) | 15873 (380) | 15953 (270) | 15775 (156) | 15954 (274) | 15932 (224) | 15775 (156) | 15954 (274) | 15932 (224) | 15932 (224) | 1 | 14097 |
| Mn | 867.4 (21.7) | 872.9 (12.0) | 852.6 (10.1) | 871.4 (14.3) | 857 (15.9) | 864.5 (11.4) | 871.4 (14.3) | 857 (15.9) | 864.5 (11.4) | 864.5 (11.4) | 1 | 863.2 |
| Co | 127.2 (1.2) | 126.4 (1.1) | 128.7 (0.8) | 130.9 (1.1) | 130.6 (1.3) | 128.6 (0.8) | 130.9 (1.1) | 130.6 (1.3) | 128.6 (0.8) | 128.6 (0.8) | 1 | 119.8 |
| Ni | 3607 (1.28) | 3587 (1.19) | 3608 (1.17) | 3567 (1.35) | 3591 (99) | 3592 (90) | 3567 (1.35) | 3591 (99) | 3592 (90) | 3592 (90) | 2 | 3689 |
| Cu | 3.061 (0.117) | 3.072 (0.115) | 3.035 (0.069) | 3.037 (0.083) | 3.034 (0.057) | 3.049 (0.068) | 3.037 (0.083) | 3.034 (0.057) | 3.049 (0.068) | 3.049 (0.068) | 2 | 2801 |
| Zn | 49.41 (0.78) | 48.85 (0.96) | 49.29 (0.82) | 50.04 (0.84) | 48.89 (0.99) | 49.26 (0.66) | 50.04 (0.84) | 48.89 (0.99) | 49.26 (0.66) | 49.26 (0.66) | 1 | 48.30 |
| Ga | 0.478 (0.034) | 0.492 (0.059) | 0.487 (0.040) | 0.463 (0.049) | 0.486 (0.021) | 0.483 (0.032) | 0.463 (0.049) | 0.486 (0.021) | 0.483 (0.032) | 0.483 (0.032) | 7 | 0.435 |
| Rb | 0.047 (0.005) | 0.048 (0.005) | 0.046 (0.001) | 0.044 (0.004) | 0.051 (0.005) | 0.047 (0.003) | 0.044 (0.004) | 0.051 (0.005) | 0.047 (0.003) | 0.047 (0.003) | 7 | 0.057 |
| Sr | 0.524 (0.038) | 0.539 (0.039) | 0.515 (0.047) | 0.536 (0.042) | 0.529 (0.027) | 0.529 (0.029) | 0.536 (0.042) | 0.529 (0.027) | 0.529 (0.029) | 0.529 (0.029) | 5 | 0.528 |
| Y | 0.029 (0.002) | 0.031 (0.003) | 0.035 (0.006) | 0.027 (0.002) | 0.023 (0.003) | 0.030 (0.003) | 0.027 (0.002) | 0.023 (0.003) | 0.030 (0.003) | 0.030 (0.003) | 9 | 0.042 |
| Zr | 0.394 (0.022) | 0.374 (0.025) | 0.383 (0.046) | 0.392 (0.036) | 0.381 (0.026) | 0.384 (0.024) | 0.392 (0.036) | 0.381 (0.026) | 0.384 (0.024) | 0.384 (0.024) | 6 | 0.203 |
| Nb | 0.028 (0.004) | 0.027 (0.005) | 0.025 (0.004) | 0.030 (0.004) | 0.025 (0.002) | 0.027 (0.003) | 0.030 (0.004) | 0.025 (0.002) | 0.027 (0.003) | 0.027 (0.003) | 10 | 0.000 |
| Ba | 12.08 (0.30) | 11.94 (0.52) | 11.85 (0.48) | 12.17 (0.47) | 12.22 (0.45) | 12.03 (0.34) | 12.17 (0.47) | 12.22 (0.45) | 12.03 (0.34) | 12.03 (0.34) | 3 | 12.54 |
| La | 0.012 (0.001) | 0.014 (0.001) | 0.012 (0.001) | 0.015 (0.002) | 0.013 (0.001) | 0.013 (0.001) | 0.015 (0.002) | 0.013 (0.001) | 0.013 (0.001) | 0.013 (0.001) | 8 | 0.015 |
| Ce | 0.019 (0.002) | 0.020 (0.003) | 0.019 (0.001) | 0.021 (0.004) | 0.019 (0.003) | 0.020 (0.002) | 0.021 (0.004) | 0.019 (0.003) | 0.020 (0.002) | 0.020 (0.002) | 11 | 0.030 |
| Pr | 0.0030 (0.0005) | 0.0028 (0.0005) | 0.0027 (0.0004) | 0.0032 (0.0005) | 0.0026 (0.0003) | 0.0029 (0.0003) | 0.0032 (0.0005) | 0.0026 (0.0003) | 0.0029 (0.0003) | 0.0029 (0.0003) | 11 | 0.0039 |
| Nd | 0.013 (0.001) | 0.014 (0.002) | 0.013 (0.001) | 0.013 (0.001) | 0.015 (0.002) | 0.014 (0.001) | 0.013 (0.001) | 0.015 (0.002) | 0.014 (0.001) | 0.014 (0.001) | 8 | 0.019 |

Table 6 (continued).
Trace element contents (in $\mu\text{g g}^{-1}$) in PCC-1 and DTS-2B from this study

| Element | DTS-2B | | | | | | | Solution ICP-MS |
|---------|------------------|-------------------|-------------------|-----------------|-----------------|-----------------|----|--------------------|
| | LA-ICP-MS | | | B 14 n = 8 | Mean, n = 46 | % RSD | | |
| | B07 | | | | | | | |
| | Slice 1 n = 8 | Slice 2 n = 12 | Slice 3 n = 10 | | | | | |
| Sm | 0.0033 (0.0007) | 0.0028 (0.0005) | 0.0028 (0.0003) | 0.0032 (0.0005) | 0.0033 (0.0004) | 0.0030 (0.0004) | 12 | 0.0031 |
| Eu | 0.0023 (0.0006) | 0.0022 (0.0003) | 0.0026 (0.0006) | 0.0025 (0.0002) | 0.0027 (0.0005) | 0.0025 (0.0004) | 14 | 0.0023 |
| Gd | 0.0051 (0.0014) | 0.0058 (0.0013) | 0.0048 (0.0015) | 0.0062 (0.0012) | 0.0047 (0.0008) | 0.0053 (0.0009) | 17 | 0.0038 |
| Tb | 0.0010 (0.0002) | 0.0012 (0.0003) | 0.0013 (0.0002) | 0.0008 (0.0002) | 0.0012 (0.0003) | 0.0011 (0.0002) | 17 | 0.0009 |
| Dy | 0.0048 (0.0009) | 0.0048 (0.0006) | 0.0055 (0.0009) | 0.0046 (0.0006) | 0.0051 (0.0008) | 0.0050 (0.0006) | 12 | 0.0043 |
| Ho | 0.0014 (0.0003) | 0.0011 (0.0002) | 0.0015 (0.0004) | 0.0014 (0.0002) | 0.0013 (0.0003) | 0.0013 (0.0002) | 16 | 0.0014 |
| Er | 0.0070 (0.0016) | 0.0063 (0.0011) | 0.0066 (0.0006) | 0.0074 (0.0008) | 0.0060 (0.0013) | 0.0066 (0.0009) | 13 | 0.0063 |
| Tm | 0.0018 (0.0004) | 0.0019 (0.0004) | 0.0015 (0.0003) | 0.0016 (0.0003) | 0.0022 (0.0005) | 0.0018 (0.0003) | 16 | 0.0011 |
| Yb | 0.011 (0.002) | 0.011 (0.002) | 0.010 (0.001) | 0.013 (0.002) | 0.014 (0.004) | 0.012 (0.002) | 15 | 0.011 |
| Lu | 0.0038 (0.0007) | 0.0033 (0.0006) | 0.0041 (0.0007) | 0.0036 (0.0005) | 0.0039 (0.0004) | 0.0037 (0.0004) | 12 | 0.0028 |
| Hf | 0.0069 (0.0015) | 0.0062 (0.0013) | 0.0073 (0.0014) | 0.0074 (0.0012) | 0.0062 (0.0010) | 0.0068 (0.0010) | 14 | 0.0056 |
| Ta | 0.0024 (0.0004) | 0.0018 (0.0005) | 0.0022 (0.0004) | 0.0023 (0.0003) | 0.0027 (0.0005) | 0.0022 (0.0003) | 15 | 0.0016 |
| Pb | 3.867 (0.241) | 3.911 (0.193) | 3.843 (0.141) | 4.063 (0.252) | 3.778 (0.157) | 3.892 (0.151) | 4 | 4.202 |
| Th | 0.0036 (0.0009) | 0.0041 (0.0005) | 0.0034 (0.0006) | 0.0038 (0.0006) | 0.0040 (0.0006) | 0.0038 (0.0005) | 13 | 0.0042 |
| U | 0.0022 (0.0006) | 0.0025 (0.0006) | 0.0020 (0.0005) | 0.0018 (0.0004) | 0.0023 (0.0005) | 0.0022 (0.0004) | 18 | 0.0024 |

Numbers in brackets are one standard deviation of the mean of multiple analyses.

Table 7.
Comparison of trace element mass fractions (in $\mu\text{g g}^{-1}$) of three natural peridotite samples obtained by the fusion method with those by solution ICP-MS

| Element | 16BY-01 | | | 15PSS-03 | | | 15TS-03 | | |
|---------|-----------------|----------------------------|---------------------|-----------------|---------------------------|---------------------|-----------------|----------------------------|---------------------|
| | Solution ICP-MS | LA-ICP-MS <i>n</i> = 12 | RD (%) ^a | Solution ICP-MS | LA-ICP-MS <i>n</i> = 8 | RD (%) ^a | Solution ICP-MS | LA-ICP-MS <i>n</i> = 10 | RD (%) ^a |
| Sc | 7.94 | 8.24 (0.47) | 3.8 | 12.6 | 12.9 (0.6) | 2.1 | 9.67 | 9.52 (0.39) | -1.5 |
| Ti | 219 | 225 (8) | 2.7 | 690 | 682 (14) | -1.2 | 486 | 493 (11) | 1.4 |
| V | 45.9 | 46.1 (1.0) | 0.4 | 77.2 | 78.8 (1.2) | 2.2 | 64.5 | 65.1 (0.7) | 0.9 |
| Cr | 2503 | 2492 (44) | -0.4 | 2403 | 2424 (43) | 0.9 | 2106 | 2137 (50) | 1.5 |
| Mn | 793 | 816 (36) | 2.9 | 865 | 853 (24) | -1.4 | 751 | 732 (33) | -2.5 |
| Co | 102 | 104 (2) | 1.9 | 107 | 104 (2) | -2.7 | 100 | 96.1 (1.5) | -3.9 |
| Ni | 2093 | 2089 (89) | -0.2 | 2050 | 2112 (101) | 3.0 | 1968 | 1926 (71) | -2.1 |
| Cu | 7.6 | 7.83 (0.32) | 3.0 | 32.1 | 32.9 (1.0) | 2.5 | 20.5 | 21.2 (0.5) | 3.4 |
| Zn | 47.8 | 51.7 (1.9) | 8.2 | 57.0 | 59.7 (2.2) | 4.7 | 50.2 | 48.8 (1.2) | -2.8 |
| Ga | 1.9 | 1.84 (0.08) | -0.8 | 7.46 | 7.50 (0.36) | 0.5 | 2.75 | 2.91 (0.08) | 6.0 |
| Rb | 0.8 | 0.80 (0.04) | -1.1 | 3.59 | 3.70 (0.09) | 3.3 | 1.53 | 1.45 (0.06) | -5.4 |
| Sr | 239 | 234 (6) | -2.2 | 21.2 | 20.0 (0.7) | -5.5 | 27.2 | 27.5 (0.5) | 1.3 |
| Y | 1.09 | 1.19 (0.04) | 9.2 | 2.90 | 2.77 (0.16) | -4.5 | 1.94 | 2.09 (0.11) | 8.1 |
| Zr | 7.35 | 7.02 (0.29) | -4.5 | 7.24 | 6.86 (0.36) | -5.2 | 4.99 | 5.15 (0.23) | 3.2 |
| Nb | 1.18 | 1.25 (0.05) | 5.8 | 0.31 | 0.31 (0.03) | -2.0 | 0.07 | 0.08 (0.01) | 16 |
| Ba | 6.28 | 6.60 (0.22) | 5.2 | 0.67 | 0.64 (0.03) | -3.2 | 1.28 | 1.23 (0.09) | -3.6 |
| La | 1.44 | 1.59 (0.07) | 11 | 0.87 | 0.82 (0.07) | -5.3 | 0.86 | 0.81 (0.04) | -5.8 |
| Ce | 3.10 | 3.34 (0.18) | 7.6 | 1.61 | 1.68 (0.13) | 4.3 | 1.74 | 1.84 (0.09) | 5.5 |
| Pr | 0.33 | 0.32 (0.02) | -2.0 | 0.19 | 0.21 (0.01) | 8.5 | 0.19 | 0.21 (0.02) | 5.8 |
| Nd | 1.53 | 1.66 (0.14) | 8.7 | 0.68 | 0.71 (0.08) | 4.3 | 0.89 | 0.96 (0.08) | 7.8 |
| Sm | 0.32 | 0.31 (0.03) | -1.9 | 0.34 | 0.34 (0.02) | -0.4 | 0.29 | 0.26 (0.02) | -13 |
| Eu | 0.09 | 0.10 (0.01) | 7.7 | 0.09 | 0.09 (0.01) | -7.9 | 0.09 | 0.09 (0.01) | -1.9 |
| Gd | 0.20 | 0.22 (0.02) | 12 | 0.42 | 0.46 (0.03) | 7.9 | 0.31 | 0.33 (0.03) | 3.8 |
| Tb | 0.04 | 0.04 (0.01) | 5.2 | 0.06 | 0.05 (0.01) | -14 | 0.05 | 0.05 (0.00) | 16 |
| Dy | 0.29 | 0.30 (0.02) | 3.9 | 0.53 | 0.47 (0.05) | -12 | 0.39 | 0.40 (0.04) | 1.9 |
| Ho | 0.05 | 0.05 (0.01) | -6.1 | 0.13 | 0.14 (0.01) | 2.9 | 0.07 | 0.06 (0.01) | -6.9 |
| Er | 0.15 | 0.16 (0.02) | 8.6 | 0.40 | 0.35 (0.03) | -14 | 0.28 | 0.28 (0.01) | -0.6 |
| Tm | 0.02 | 0.02 (0.00) | 4.4 | 0.05 | 0.04 (0.00) | -12 | 0.03 | 0.03 (0.00) | 16 |
| Yb | 0.10 | 0.12 (0.01) | 16 | 0.32 | 0.34 (0.03) | 6.1 | 0.21 | 0.18 (0.02) | -12 |
| Lu | 0.01 | 0.01 (0.00) | -21 | 0.06 | 0.05 (0.01) | -14 | 0.05 | 0.04 (0.01) | -14 |
| Hf | 0.18 | 0.20 (0.02) | 9.0 | 0.18 | 0.20 (0.02) | 16 | 0.14 | 0.12 (0.02) | -12 |
| Ta | 0.06 | 0.06 (0.01) | 7.5 | 0.01 | 0.01 (0.00) | 7.1 | 0.02 | 0.02 (0.00) | 7.3 |
| Pb | 0.18 | 0.16 (0.01) | -9.0 | 0.25 | 0.27 (0.01) | 11 | 0.16 | 0.17 (0.00) | 2.4 |
| Th | 0.13 | 0.12 (0.01) | -9.6 | 0.10 | 0.11 (0.01) | 20 | 0.13 | 0.14 (0.02) | 4.9 |
| U | 0.06 | 0.06 (0.00) | 1.1 | 0.05 | 0.04 (0.00) | -13 | 0.03 | 0.03 (0.00) | 10 |

Numbers in brackets are one standard deviation of the mean of multiple analyses.

^a RD (relative deviation) (%) = $100 \times (\text{LA-ICP-MS measured values} - \text{solution ICP-MS measured values}) / \text{solution ICP-MS measured values}$.

is accurate and robust. This provides an independent test for the reliability of our albite fusion method.

Three peridotite samples (16BY-01, 15PSS-03 and 15TS-03) were analysed to further test the reliability of the method combining albite fusion and LA-ICP-MS. The results for the natural samples using albite fusion and conventional acid digestion are compared in Table 7. The RSD of element mass fractions of 16BY-01, 15PSS-03 and 15TS-03 using the albite fusion method are generally smaller than 10% (Figure 7a) except for those of REE, Ta, Hf, Th and U, which are slightly larger than 10%. We attribute the latter to low mass fractions of the peridotites. At the same time, the data for most elements (except REE, Ta, Hf, Pb, Th and U)

and U) obtained with the albite fusion method in the three samples are consistent with solution ICP-MS results within a small variation range of 10% (Figure 7b). Overall, these observations suggest that the albite fusion method can provide trace element mass fractions for the majority of elements in this study (except REE, Ta, Hf, Pb, Th and U) at adequate precision and accuracy.

In summary, the results obtained on both the reference materials and natural peridotites indicate that the albite fusion method can yield accurate trace element mass fractions, especially for the first series transition elements, LILE and Zr in peridotites with precision comparable to the conventional solution ICP-MS method.

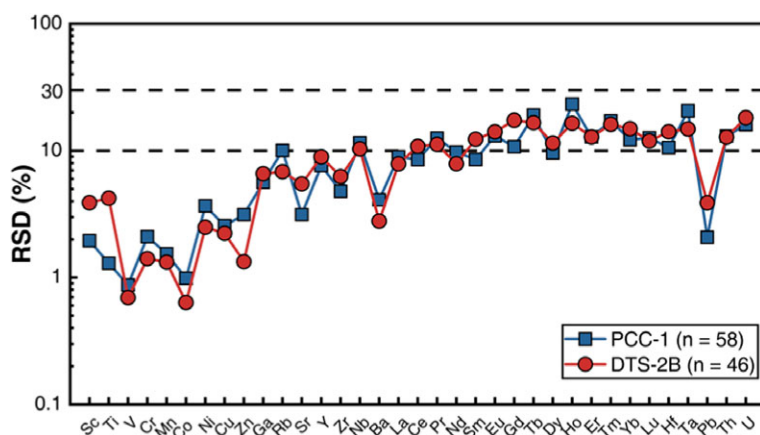


Figure 5. RSD of trace element mass fractions in USGS reference materials PCC-1 and DTS-2B obtained from the new method in this study.

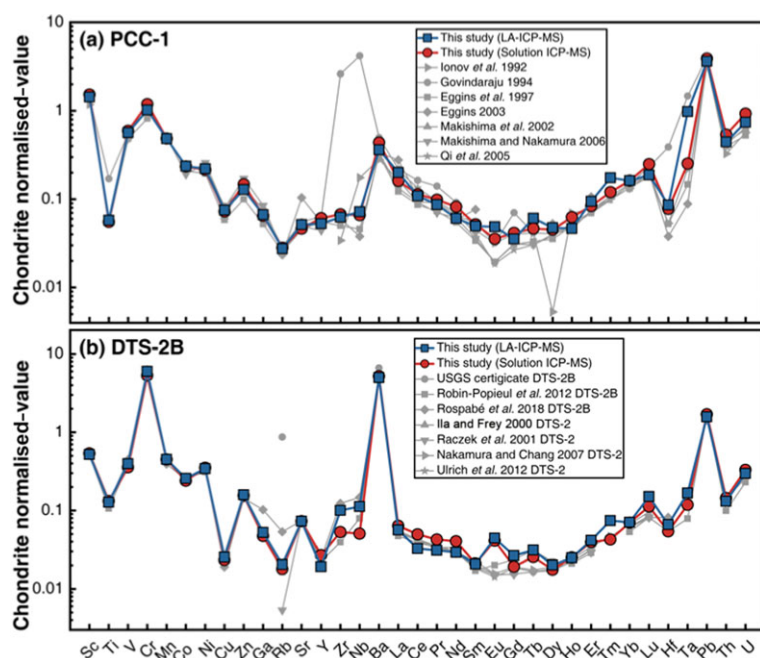


Figure 6. Chondrite-normalised (McDonough and Sun 1995) trace element patterns in this study for (a) PCC-1 and (b) DTS-2B compared with those from previous work (Ionov *et al.* 1992, Govindaraju 1994, Eggins *et al.* 1997, Ila and Frey 2000, Raczek *et al.* 2001, Makishima *et al.* 2002, Eggins 2003, Qi *et al.* 2005, Makishima and Nakamura 2006, Nakamura and Chang 2007, Robin-Popieul *et al.* 2012, Ulrich *et al.* 2012). All experiments were performed at optimum conditions (1500 °C, 10 min and SFR of 1:2). Results are compared with literature values as labelled and listed in Table S3.

Conclusions

This study developed a novel sample fusion method for time- and cost-efficient analysis of trace element compositions of peridotites using LA-ICP-MS. We use a heated molybdenum–graphite assembly to fuse rock powders with synthetic albite and obtain homogeneous glasses for *in situ*

analyses with LA-ICP-MS and potentially other microbeam techniques. After mixing with synthetic albite with sample-to-flux ratio (SFR) of 1:2, two USGS reference materials, PCC-1 (peridotite) and DTS-2B (dunite), were melted at 1500–1550 °C for 10–15 min in a one-atmosphere furnace and quenched to homogeneous glasses. The method allows quick and accurate measurement of many trace elements in

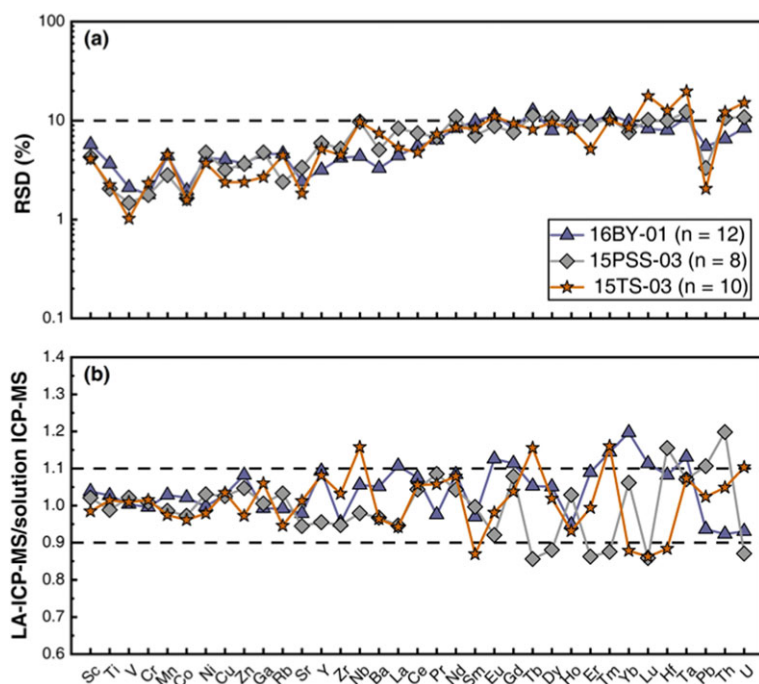


Figure 7. (a) RSD of element mass fractions in 16BY-01, 15PSS-03 and 15TS-03 using LA-ICP-MS and the fusion method in this study (synthesised at 1500 °C for 10 min with SFR of 1:2); (b) comparison of elemental mass fractions obtained from LA-ICP-MS in this study with conventional solution ICP-MS.

the quenched glass, especially the first series transition elements (Sc, Ti, V, Cr, Mn, Co, Ni, Cu and Zn), some of which are concentrated in spinel and other acid-resistant minerals, and may be underestimated by methods using conventional acid digestion. First series transition element mass fraction obtained for two USGS reference materials and three natural peridotites agree well with published data and solution ICP-MS method within 10%. Therefore, the albite fusion method can be applied to rapidly and accurately determine trace element mass fractions in peridotites, in particular for many elements residing in acid-resistant minerals.

Acknowledgements

We thank Editor Paul J. Sylvester and two anonymous reviewers for their insightful comments and constructive criticism that greatly improved the quality of this paper. We thank Ying Xia and Zhiwei He for assistance during flux agent preparation, Mei Xia for assistance on the SEM imaging, Yerong Jiang for preparation of Mo-graphite assembly and Jian Huang for providing the natural powdered samples. This study was supported by the National Key R&D Program of China (No. 2016YFC0600404) from Ministration of Science and Technology of China, the National Science Foundation

of China (grants 41630206, 41573017, and 41603058), China Postdoctoral Science Foundation (BH2080000065) to H.L. Zhang and the Visiting Scientist fellowship within the CAS (Chinese Academy of Sciences) President's International Fellowship Initiative (PIFI) to D.A. Ionov in 2017–18.

References

- Bao Z., Zhang H., Yuan H., Liu Y., Chen K. and Zong C. (2016) Flux-free fusion technique using a boron nitride vessel and rapid acid digestion for determination of trace elements by ICP-MS. *Journal of Analytical Atomic Spectrometry*, 31, 2261–2271.
- Barrat J.A., Keller F., Amossé J., Taylor R.N., Nesbitt R.W. and Hirata T. (1996) Determination of rare earth elements in sixteen silicate reference samples by ICP-MS after Tm addition and ion exchange separation. *Geostandards Newsletter*, 20, 133–139.
- Bayon G., Barrat J.A., Etoubleau J., Benoit M., Bollinger C. and Révillon S. (2009) Determination of rare earth elements, Sc, Y, Zr, Ba, Hf and Th in geological samples by ICP-MS after Tm addition and alkaline fusion. *Geostandards and Geoanalytical Research*, 33, 51–62.

references

- Bodinier J.L. and Godard M. (2014)**
Orogenic, ophiolitic, and abyssal peridotites. In: Carlson R.W. (ed.), *Treatise on geochemistry* (2nd edition). Elsevier (Oxford), 103–167.
- Bokhari S.N.H. and Meisel T.C. (2017)**
Method development and optimisation of sodium peroxide sintering for geological samples. *Geostandards and Geoanalytical Research*, 41, 181–195.
- Canil D. (2002)**
Vanadium in peridotites, mantle redox and tectonic environments: Archean to present. *Earth and Planetary Science Letters*, 195, 75–90.
- Carswell D.A. (1968)**
Possible primary upper mantle peridotite in Norwegian basal gneiss. *Lithos*, 1, 322–355.
- Chen L., Liu Y.S., Hu Z.S., Gao S., Zong K.Q. and Chen H.H. (2011)**
Accurate determinations of fifty-four major and trace elements in carbonate by LA-ICP-MS using normalization strategy of bulk components as 100%. *Chemical Geology*, 284, 283–295.
- Cotta A.J.B. and Enzweiler J. (2012)**
Classical and new procedures of whole rock dissolution for trace element determination by ICP-MS. *Geostandards and Geoanalytical Research*, 36, 27–50.
- Day J.M.D., Barry P.H., Hilton D.R., Burgess R., Pearson D.G. and Taylor L.A. (2015)**
The helium flux from the continents and ubiquity of low-³He/⁴He recycled crust and lithosphere. *Geochimica et Cosmochimica Acta*, 153, 116–133.
- Eggins S.M. (2003)**
Laser ablation ICP-MS analysis of geological materials prepared as lithium borate glasses. *Geostandards Newsletter: The Journal of Geostandards and Geoanalysis*, 27, 147–162.
- Eggins S.M., Woodhead J.D., Kinsley L.P.J., Mortimer G.E., Sylvester P., McCulloch M.T., Hergt J.M. and Handler M.R. (1997)**
A simple method for the precise determination of ≥ 40 trace elements in geological samples by ICP-MS using enriched isotope internal standardisation. *Chemical Geology*, 134, 311–326.
- Fedorowich J.S., Richards J.P., Jain J.C., Kerrich R. and Fan J. (1993)**
A rapid method for REE and trace-element analysis using laser sampling ICP-MS on direct fusion whole-rock glasses. *Chemical Geology*, 106, 229–249.
- Flanagan F.J. (1967)**
US Geological Survey silicate rock standards. *Geochimica et Cosmochimica Acta*, 31, 289–308.
- Foley S., Massimo T. and Riccardo V. (2002)**
Growth of early continental crust controlled by melting of amphibolite in subduction zones. *Nature*, 417, 837–840.
- Frey F.A. and Prinz M. (1978)**
Ultramafic inclusions from San Carlos, Arizona: Petrologic and geochemical data bearing on their petrogenesis. *Earth and Planetary Science Letters*, 38, 129–176.
- Garbe-Schönberg D. and Müller S. (2014)**
Nano-particulate pressed powder tablets for LA-ICP-MS. *Journal of Analytical Atomic Spectrometry*, 29, 990–1000.
- Govindaraju K. (1994)**
1994 compilation of working values and sample description for 383 geostandards. *Geostandards Newsletter*, 18 (Special Issue), 158pp.
- Gray A.L. (1985)**
Solid sample introduction by laser ablation for inductively coupled plasma source mass spectrometry. *Analyst*, 110, 551–556.
- Günther D. and Hattendorf B. (2005)**
Solid sample analysis using laser ablation inductively coupled plasma-mass spectrometry. *TrAC Trends in Analytical Chemistry*, 24, 255–265.
- He Z., Huang F., Yu H., Xiao Y., Wang F., Li Q., Xia Y. and Zhang X. (2016)**
A flux-free fusion technique for rapid determination of major and trace elements in silicate rocks by LA-ICP-MS. *Geostandards and Geoanalytical Research*, 40, 5–21.
- Herzberg C.T. (1983)**
Solidus and liquidus temperatures and mineralogies for anhydrous garnet-lherzolite to 15 GPa. *Physics of the Earth and Planetary Interiors*, 32, 193–202.
- Herzberg C., Asimow P.D., Ionov D.A., Vidito C., Jackson M.G. and Geist D. (2013)**
Nickel and helium evidence for melt above the core-mantle boundary. *Nature*, 493, 393–397.
- Hou Z. and Wang C. (2007)**
Determination of 35 trace elements in geological samples by inductively coupled plasma-mass spectrometry. *Journal of University of Science and Technology of China*, 37, 940–944.
- Ila P. and Frey F.A. (2000)**
Trace element analysis of USGS standards AGV2, BCR2, BHVO2, DTS2 and GSP2 by INAA. *Journal of Radioanalytical and Nuclear Chemistry*, 244, 599–602.
- Ionov D.A., Savoyant L. and Dupuy C. (1992)**
Application of the ICP-MS technique to trace element analysis of peridotites and their minerals. *Geostandards Newsletter*, 16, 311–315.
- Ionov D.A., Grégoire M. and Prikhod'ko V.S. (1999)**
Feldspar-Ti-oxide metasomatism in off-cratonic continental and oceanic upper mantle. *Earth and Planetary Science Letters*, 165, 37–44.



references

Ionov D.A., Bodinier J.-L., Mukasa S.B. and Zanetti A. (2002)

Mechanisms and sources of mantle metasomatism: Major and trace element compositions of peridotite xenoliths from Spitsbergen in the context of numerical modeling. *Journal of Petrology*, 43, 2219–2259.

Jarvis I. (1992)

Sample preparation for ICP-MS. In: Jarvis K.E., Gray A.L. and Houk R.S. (eds), *Handbook of inductively coupled plasma-mass spectrometry*. Blackie (Glasgow), 172–224.

Jenner G.A., Longerich H.P., Jackson S.E. and Fryer B.J. (1990)

ICP-MS – A powerful tool for high-precision trace-element analysis in Earth sciences: Evidence from analysis of selected U.S.G.S. reference samples. *Chemical Geology*, 83, 133–148.

Kawaguchi H., Tanaka T., Nakamura T., Morishita M. and Mizuike A. (1987)

Matrix effects in inductively coupled plasma-mass spectrometry. *Analytical Science*, 3, 305–308.

Kent A.J.R. and Ungerer C.A.A. (2005)

Production of barium and light rare earth element oxides during LA-ICP-MS microanalysis. *Journal of Analytical Atomic Spectrometry*, 20, 1256–1262.

Klemme S., Günther D., Hametner K., Prowatke S. and Zack T. (2006)

The partitioning of trace elements between ilmenite, ulvospinel, armalcolite and silicate melts with implications for the early differentiation of the moon. *Chemical Geology*, 234, 251–263.

Kurosawa M., Shima K., Ishii S. and Sasa K. (2006)

Trace element analysis of fused whole-rock glasses by laser ablation-ICP-MS and PIXE. *Geostandards and Geoanalytical Research*, 30, 17–30.

Liu Y., Hu Z., Gao S., Günther D., Xu J., Gao C. and Chen H. (2008)

In situ analysis of major and trace elements of anhydrous minerals by LA-ICP-MS without applying an internal standard. *Chemical Geology*, 257, 34–43.

Longerich H.P., Jackson S.E. and Günther D. (1996)

Inter-laboratory note. Laser ablation inductively coupled plasma-mass spectrometric transient signal data acquisition and analyte concentration calculation. *Journal of Analytical Atomic Spectrometry*, 11, 899–904.

Makishima A. and Nakamura E. (1997)

Suppression of matrix effects in ICP-MS by high power operation of ICP. Application to precise determination of Rb, Sr, Y, Cs, Ba, REE, Pb, Th and U at ng g⁻¹ levels in milligram silicate samples. *Geostandards Newsletter: The Journal of Geostandards and Geoanalysis*, 21, 307–319.

Makishima A. and Nakamura E. (2006)

Determination of major, minor and trace elements in silicate samples by ICP-QMS and ICP-SFMS applying isotope dilution-internal standardisation (ID-IS) and multi-stage internal standardisation. *Geostandards and Geoanalytical Research*, 30, 245–271.

Makishima A., Kobayashi K. and Nakamura E. (2002)

Determination of chromium, nickel, copper and zinc in milligram samples of geological materials using isotope dilution high resolution inductively coupled plasma-mass spectrometry. *Geostandards Newsletter: The Journal of Geostandards and Geoanalysis*, 26, 41–51.

McDonough W.F. (1990)

Constraints on the composition of the continental lithospheric mantle. *Earth and Planetary Science Letters*, 101, 1–18.

McDonough W.F. and Sun S.-S. (1995)

The composition of the Earth. *Chemical Geology*, 120, 223–253.

Meisel T., Schöner N., Paliulionyte V. and Kahr E. (2002)

Determination of rare earth elements, Y, Th, Zr, Hf, Nb and Ta in geological reference materials G-2, G-3, SC0-1 and WGB-1 by sodium peroxide sintering and inductively coupled plasma-mass spectrometry. *Geostandards Newsletter: The Journal of Geostandards and Geoanalysis*, 26, 53–61.

Mukherjee P.K., Khanna P.P. and Saini N.K. (2014)

Rapid determination of trace and ultra-trace level elements in diverse silicate rocks in pressed powder pellet targets by LA-ICP-MS using a matrix independent protocol. *Geostandards and Geoanalytical Research*, 38, 363–379.

Nakamura K. and Chang Q. (2007)

Precise determination of ultra-low (sub-ng g⁻¹) level rare earth elements in ultramafic rocks by quadrupole ICP-MS. *Geostandards and Geoanalytical Research*, 31, 185–197.

Pearson D.G., Canil D. and Shirey S.B. (2014)

Mantle samples included in volcanic rocks: Xenoliths and diamonds. In: Carlson R.W. (ed.), *Treatise on geochemistry* (2nd edition). Elsevier (Oxford), 169–253.

Peters D. and Pettke T. (2017)

Evaluation of major to ultra trace element bulk rock chemical analysis of nanoparticulate pressed powder pellets by LA-ICP-MS. *Geostandards and Geoanalytical Research*, 41, 5–28.

Qi L., Zhou M., Malpas J. and Sun M. (2005)

Determination of rare earth elements and Y in ultramafic rocks by ICP-MS after pre-concentration using Fe(OH)₃ and Mg(OH)₂ co-precipitation. *Geostandards and Geoanalytical Research*, 29, 131–141.

Raczek I., Stoll B., Hofmann A.W. and Jochum K.P. (2001)

High-precision trace element data for the USGS reference materials BCR-1, BCR-2, BHVO-1, BHVO-2, AGV-1, AGV-2, DTS-1, DTS-2, GSP-1 and GSP-2 by ID-TIMS and MIC-SSMS. *Geostandards Newsletter: The Journal of Geostandards and Geoanalysis*, 25, 77–86.

Rampone E., Hofmann A.W., Piccardo G.B., Vannucci R., Bottazzi P. and Ottolini L. (1996)

Trace element and isotope geochemistry of depleted peridotites from an N-MORB type ophiolite (Internal Liguride, N. Italy). *Contributions to Mineralogy and Petrology*, 123, 61–76.

references

Reading D.G., Croudace I.W. and Warwick P.E. (2017)
Fusion bead procedure for nuclear forensics employing synthetic enstatite to dissolve uraniferous and other challenging materials prior to laser ablation inductively coupled plasma-mass spectrometry. *Analytical Chemistry*, **89**, 6006–6014.

Regnery J., Stoll B. and Jochum K.P. (2010)
High-resolution LA-ICP-MS for accurate determination of low abundances of K, Sc and other trace elements in geological samples. *Geostandards and Geoanalytical Research*, **34**, 19–38.

Robin-Popieul C.C.M., Arndt N.T., Chauvel C., Byerly G.R., Sobolev A.V. and Wilson A. (2012)
A new model for Barberton komatiites: Deep critical melting with high melt retention. *Journal of Petrology*, **53**, 2191–2229.

Rospabé M., Benoit M. and Candaudap F. (2018)
Determination of trace element mass fractions in ultramafic rocks by HR-ICP-MS: A combined approach using a direct digestion/dilution method and pre-concentration by coprecipitation. *Geostandards and Geoanalytical Research*, **42**, 115–129.

Stoll B., Jochum K.P., Herwig K., Amini M., Flanz M., Kreuzburg B., Kuzmin D., Willbold M. and Enzweiler J. (2008)
An automated iridium-strip heater for LA-ICP-MS bulk analysis of geological samples. *Geostandards and Geoanalytical Research*, **32**, 5–26.

Sun Y., Sun S., Wang C.Y. and Xu P. (2013)
Determination of rare earth elements and thorium at nanogram levels in ultramafic samples by inductively coupled plasma-mass spectrometry combined with chemical separation and preconcentration. *Geostandards and Geoanalytical Research*, **37**, 65–76.

Tabersky D., Luechinger N.A., Rossier M., Reusser E., Hametner K., Aeschlimann B., Frick D.A., Halim S.C., Thompson J. and Danyushevsky L. (2014)
Development and characterization of custom-engineered and compacted nanoparticles as calibration materials for quantification using LA-ICP-MS. *Journal of Analytical Atomic Spectrometry*, **29**, 955–962.

Takahashi E. and Kushiro I. (1983)
Melting of a dry peridotite at high pressures and basalt magma genesis. *American Mineralogist*, **68**, 859–879.

Ulrich M., Bureau S., Chauvel C. and Picard C. (2012)
Accurate measurement of rare earth elements by ICP-MS after ion-exchange separation: Application to ultra-depleted samples. *Geostandards and Geoanalytical Research*, **36**, 7–20.

Xiao Y., Zhang H.F., Fan W.M., Ying J.F., Zhang J., Zhao X.M. and Su B.X. (2010)
Evolution of lithospheric mantle beneath the Tan–Lu fault zone, eastern North China Craton: Evidence from petrology and geochemistry of peridotite xenoliths. *Lithos*, **117**, 229–246.

Yokoyama T., Makishima A. and Nakamura E. (1999)
Evaluation of the coprecipitation of incompatible trace elements with fluoride during silicate rock dissolution by acid digestion. *Chemical Geology*, **157**, 175–187.

Yu Z., Norman M.D. and Robinson P. (2003)
Major and trace element analysis of silicate rocks by XRF and laser ablation ICP-MS using lithium borate fused glasses: Matrix effects, instrument response and results for international reference materials. *Geostandards Newsletter: The Journal of Geostandards and Geoanalysis*, **27**, 67–89.

Zeng G., Chen L.H., Xu X.S., Hu S.L. and Yang L.F. (2013)
Genesis of Cenozoic low-Ca alkaline basalts in the Nanjing basaltic field, eastern China: The case for mantle xenolith-magma interaction. *Geochemistry Geophysics Geosystems*, **14**, 1660–1677.

Zhang C., Hu Z., Zhang W., Liu Y., Zong K., Li M., Chen H. and Hu S. (2016)
Green and fast laser fusion technique for bulk silicate rock analysis by laser ablation-inductively coupled plasma-mass spectrometry. *Analytical Chemistry*, **88**, 10088–10094.

Zhu L., Liu Y., Hu Z., Hu Q., Tong X., Zong K., Chen H. and Gao S. (2013a)
Simultaneous determination of major and trace elements in fused volcanic rock powders using a hermetic vessel heater and LA-ICP-MS. *Geostandards and Geoanalytical Research*, **37**, 207–229.

Zhu Y., Hioki A. and Chiba K. (2013b)
Quantitative analysis of the elements in powder samples by LA-ICP-MS with PMMA powder as the binder and Cs as the internal standard. *Journal of Analytical Atomic Spectrometry*, **28**, 301–306.

Supporting information

The following supporting information may be found in the online version of this article:

Table S1. Mass fractions of trace elements in secondary reference materials TB-1G and GSD-1G calibrated using the *MRM-NoIS* approach compared with reference values.

Table S2. Trace element mass fractions in ‘external’ standard solutions.

Table S3. Literature values of trace element contents in PCC-1 and DTS-2B.

This material is available from: <http://onlinelibrary.wiley.com/doi/10.1111/ggr.12240/abstract>. (This link will take you to the article abstract.)



